

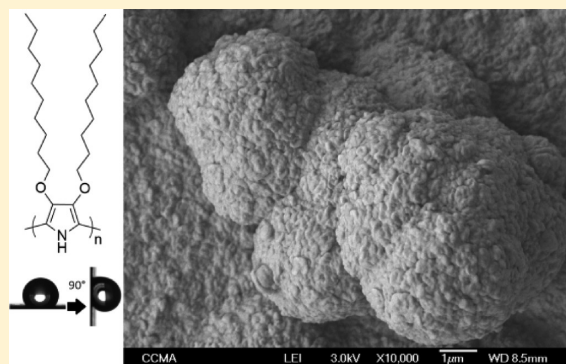
3,4-Dialkoxypyrrole for the Formation of Bioinspired Rose Petal-like Substrates with High Water Adhesion

Claudio Mortier, Thierry Darmanin, and Frédéric Guittard*

Université Nice Sophia Antipolis, CNRS, LPMC, UMR 7336, 06100 Nice, France

Supporting Information

ABSTRACT: Self-organization is commonly present in nature and can lead to the formation of surface structures with different wettabilities. Indeed, in nature superhydrophobic (low water adhesion) and parahydrophobic (high water adhesion) properties exist, such as in lotus leaves and red roses, respectively. The aim of this work is to prepare parahydrophobic properties by electrodeposition. For this, pyrrole derivatives with two alkoxy groups of various lengths (from 1 to 12) were synthesized in 8 steps by adapting a method developed by Merz et al. We show that the alkyl chain length has a huge influence on the polymer solubility and as a consequence on the surface morphology and hydrophobicity. Moreover, the alkyl chain length should be at least greater than eight carbons in order to obtain parahydrophobic properties. The properties are also controlled by the electrolyte nature. These materials can be used for many potential applications in water harvesting and transportation and separation membranes.



INTRODUCTION

Self-organized systems are commonly used in solution in surfactants and membranes but can also lead to the formation of surface structures.^{1,2} As a consequence, they can be extremely useful in modifying the surface hydrophobicity. Indeed, controlling surface hydrophobicity and water adhesion is fundamental to various potential applications, for example, in cookware, self-cleaning and self-healing fabrics, antifingerprint optical devices, antibioadhesion/antibiofouling coatings, separation membranes, and sensors.^{3–6} In the literature, there are very recent developments of multifunctional structured surfaces with both special wettabilities and adhesion using different processes, and they are usually inspired by nature.^{7–10} Superhydrophobic properties, characterized by an extremely high water apparent contact angle θ_w and ultralow water adhesion or hysteresis (H), are commonly present in nature. This is the case of the famous self-cleaning lotus leaves, and these properties give a considerable advantage,¹¹ for example, against other predators. For example, flying insects possess antireflection and antifogging eyes,¹² and other insects can slide on the surface of the water with their feet.¹³ It was shown that dual-scale or fractal surface structures and materials of low surface energy are preferable to achieving superhydrophobic properties with high robustness.^{14–16}

By contrast, on other natural substrates, both extremely high θ_w and extremely strong water adhesion,^{17–23} also called parahydrophobic properties by Marmur, were observed.²⁴ This is the case of rose petals,^{17,18} peach skin,¹⁹ cicada wings²¹ and gecko feet.²⁰ Very recently, Yarger et al. also reported that embiopteran *Antipaluria urichi* weaves silk fibers into sheets having extremely strong water adhesion.²² They observed that these properties are

due to the presence of loosely woven sheets. These properties are extremely interesting, for example, in trapping small water droplet in dry environments^{25–28} and can found in many potential applications in water transportation and harvesting,²⁹ water/oil separation,³⁰ and underwater locomotion.³¹ Hence, to achieve parahydrophobic properties it is preferable to produce surface structures at only one scale (nanostructures, for example) and/or to increase the surface energy. This can be achieved using various strategies including laser treatment,³² plasma etching,³³ chemical vapor deposition,³⁴ phase separation,³⁵ colloidal lithography,³⁶ and inkjet imprinting.³⁷

Conducting polymers can also be used to control both θ_w and water adhesion. Many strategies were employed to obtain structured and organized conducting polymers.^{38–40} Among them, polyaniline was largely used in solution to obtain nanostructured polymers by self-organization.^{41,42} For example, rambutan, dandelion squares, and starlike structures were reported, and superhydrophobic properties were obtained after depositing these materials by dip-coating, spin-coating, or spray-coating. Using fluorinated doping agents, switchable surfaces from superhydrophobic to superhydrophilic were reported by a simple change in voltage.⁴³ One-step processes, where the growth of structured conducting polymers is induced directly on substrates, were also reported, including preferential growth,⁴⁴ grafting,⁴⁵

Special Issue: Tribute to Toyoki Kunitake, Pioneer in Molecular Assembly

Received: June 16, 2016

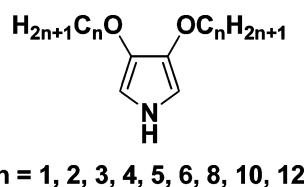
Revised: July 27, 2016

vapor-phase polymerization,⁴⁶ plasma polymerization,⁴⁷ and electropolymerization.^{48,49}

Electropolymerization is a very fast and controllable process for developing organized conducting polymer films. Here, a monomer is oxidized in an electrochemical cell to induce polymerization and polymer deposition on a working electrode.^{48,49} Different conductive substrates can be used as working electrodes, such as platinum, gold, titanium, stainless steel, and transparent conductive glass (ITO) but not aluminum because of the presence of the oxide layer. Complex substrates such as meshes can also be used because polymerization starts from the substrate. The surface structures are highly dependent on electrochemical parameters and also on the monomer structure. It was shown that 3,4-ethylenedioxyppyrrrole (EDOP) and 3,4-propylenedioxyppyrrrole (ProDOP) derivatives have unique properties in terms of polymerization capacity but also in terms of their optoelectronic^{50–54} and wetting properties. Indeed, in comparison with classical pyrrole derivatives, the presence of two alkoxy groups in the 3 and 4 positions has several advantages. First, they make polymerization possible only in the 2 and 5 positions, which greatly increases the polymer conductivity. Moreover, their presence also reduces the monomer oxidation potential by electrodonating effects. For example, fluorinated EDOP was used to develop nanoporous superoleophobic films^{55,56} and EDOP with branched alkyl chains and aromatic substituents was used to obtain parahydrophobic properties.^{57,58} However, because of the extreme difficulty in synthesizing these compounds, which are also very sensitive, the study of many of these derivatives is missing in the literature. Indeed, these derivatives are usually synthesized in eight steps from iminodiacetic using the process reported by Merz et al.⁵⁹

Among all of the derivatives that can be synthesized with this process, here we were interested in 3,4-dialkoxy-1H-pyrrole (Scheme 1: Py(OC_n)₂) with *n* = 1 to 12. If some of these deriv-

Scheme 1. Monomers Synthesized and Studied in This Article



atives were already synthesized in the literature (*n* = 1 and 2),⁵⁶ their surface properties and especially their wetting properties have never been explored. Indeed, because of the presence of free NH groups, which are very polar, it is expected to lead to high water adhesion. Here, we report for the first time a complete study of their surface morphology and wettability of as a function of the alkyl chain length (nine monomers were synthesized as shown in Scheme 1).

EXPERIMENTAL SECTION

Synthesis. All of the starting chemical compounds used in this study were purchased from Sigma-Aldrich. The monomers were synthesized in eight steps from iminodiacetic acid as shown in Scheme 2 by adapting a strategy developed by Merz et al.⁵⁹ Indeed, Merz et al. reported a process in eight steps that can be used to obtain EDOP and ProDOP but also Py(OC₁)₂ and Py(OC₂)₂. Indeed, for all of these molecules it is first necessary to synthesize diethyl 1-benzyl-3,4-dihydroxy-1H-pyrrole-2,5-dicarboxylate in four steps, and then different molecules can be envisaged using different bromides or dibromides. Here, we show also that by suppressing extraction

steps it is also possible to reach Py(OC_n)₂ with extremely long alkyl chains.

Hence, before monomer synthesis, an intermediary compound, diethyl 1-benzyl-3,4-dihydroxy-1H-pyrrole-2,5-dicarboxylate, was synthesized in four steps from iminodiacetic acid as shown in Scheme 1. Then, the monomers were obtained by nucleophilic substitution from diethyl 1-benzyl-3,4-dihydroxy-1H-pyrrole-2,5-dicarboxylate and, using different bromides, deprotection of the amine function, saponification in an acid medium, and decarboxylation on the following compounds. The monomer mass spectra and the ¹H and ¹³C spectra are available in the Supporting Information.

The synthesis process is given below.

Nucleophilic Substitution of Diethyl 1-Benzyl-3,4-dihydroxy-1H-pyrrole-2,5-dicarboxylate. To 500 mL of dimethylformamide (DMF) were added 25 g of diethyl 1-benzyl-3,4-dihydroxy-1H-pyrrole-2,5-dicarboxylate (75 mmol, 1 equiv) and 30 g of K₂CO₃ (0.2 mol, 3 equiv). The solution was stirred and held at 100 °C for 30 mn. Then, the corresponding 1-iodoalkane (for *n* = 1 to 5) or 1-bromoalkane (for *n* = 6 to 12) was added slowly (0.3 mol, 4 equiv). After 2 days at 100 °C (70 °C for *n* = 1 and 2), the product was extracted with ethyl acetate. Finally, the product was distilled at 120 °C under pressure to remove all volatile impurities. The product could be used for the next step without other treatment.

Diethyl 1-Benzyl-3,4-dimethoxy-1H-pyrrole-2,5-dicarboxylate. Yield 52.6%, brown liquid. δ_{H} (200 MHz, CDCl₃): 7.24 (3 H, m), 6.95 (2 H, d), 5.97 (2 H, s), 4.29 (4 H, q), 3.9 (6 H, s), 1.29 (6 H, t).

Diethyl 1-Benzyl-3,4-diethoxy-1H-pyrrole-2,5-dicarboxylate. Yield 89.7%, brown liquid. δ_{H} (200 MHz, CDCl₃): 7.22 (3 H, m), 6.94 (2 H, d), 5.99 (2 H, s), 4.27 (4 H, q), 4.13 (4 H, q), 1.36 (6 H, t), 1.30 (6 H, t).

Diethyl 1-Benzyl-3,4-dipropoxy-1H-pyrrole-2,5-dicarboxylate. Yield 85.6%, brown oil. δ_{H} (200 MHz, CDCl₃): 7.23 (3 H, m), 6.93 (2 H, d), 5.99 (2 H, s), 4.27 (4 H, q), 4.00 (4 H, t), 1.79 (4H, m), 1.29 (6 H, t), 1.02 (6 H, t).

Diethyl 1-Benzyl-3,4-dibutoxy-1H-pyrrole-2,5-dicarboxylate. Yield 98.3%, brown oil. δ_{H} (200 MHz, CDCl₃): 7.23 (3 H, m), 6.92 (2 H, d), 5.98 (2 H, s), 4.29 (4 H, q), 4.04 (4 H, t), 1.76 (4H, m), 1.42 (4H, m), 1.29 (6 H, t), 0.99 (6 H, t).

Diethyl 1-Benzyl-3,4-bis(pentyloxy)-1H-pyrrole-2,5-dicarboxylate. Yield 98.5%, yellow oil. δ_{H} (200 MHz, CDCl₃): 7.26 (3 H, m), 6.92 (2 H, d), 5.98 (2 H, s), 4.27 (4 H, q), 4.03 (4 H, t), 1.75 (4H, m), 1.33 (8H, m), 1.29 (6 H, t), 0.92 (6 H, t).

Diethyl 1-Benzyl-3,4-bis(hexyloxy)-1H-pyrrole-2,5-dicarboxylate. Yield 93.5%, orange oil. δ_{H} (200 MHz, CDCl₃): 7.22 (3 H, m), 6.92 (2 H, d), 5.98 (2 H, s), 4.27 (4 H, q), 4.03 (4 H, t), 1.74 (4H, m), 1.47 (4H, m), 1.43 (8 H, m), 1.31 (6 H, t), 0.93 (6 H, t).

Diethyl 1-Benzyl-3,4-bis(octyloxy)-1H-pyrrole-2,5-dicarboxylate. Yield 98.0%, orange oil. δ_{H} (200 MHz, CDCl₃): 7.22 (3 H, m), 6.93 (2 H, d), 5.98 (2 H, s), 4.27 (4 H, q), 4.02 (4 H, t), 1.77 (4H, m), 1.39 (26 H, m), 0.90 (6 H, t).

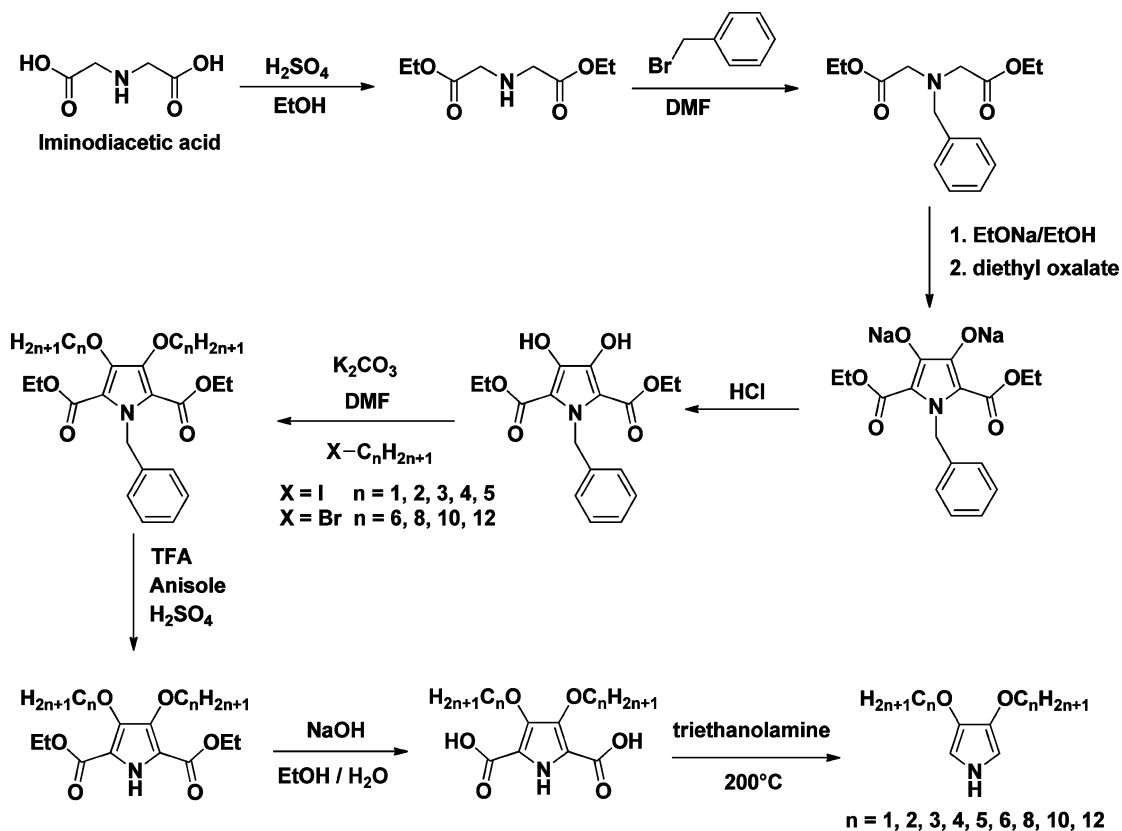
Diethyl 1-Benzyl-3,4-bis(decyloxy)-1H-pyrrole-2,5-dicarboxylate. Yield 98.0%, orange oil. δ_{H} (200 MHz, CDCl₃): 7.18 (3 H, m), 6.92 (2 H, d), 5.98 (2 H, s), 4.27 (4 H, q), 4.02 (4 H, t), 1.74 (4H, m), 1.29 (34 H, m), 0.87 (6 H, t).

Diethyl 1-Benzyl-3,4-bis(dodecyloxy)-1H-pyrrole-2,5-dicarboxylate. Yield 98%, orange oil. δ_{H} (200 MHz, CDCl₃): 7.22 (3 H, m), 6.92 (2 H, d), 5.98 (2 H, s), 4.27 (4 H, q), 4.02 (4 H, t), 1.76 (8H, m), 1.32 (38 H, m), 0.88 (6 H, t).

Deprotection of the Amine Function and Saponification in an Acidic Medium. Because the synthesis process is different for different alkyl chain lengths (*n*), we give the process for each case. For *n* ≥ 6, the extraction steps were suppressed by the amphiphilic behavior of the products.

For *n* = 1 to 5. For the deprotection of the amine, the product was dissolved in 200 mL of trifluoroacetic acid. Then, anisole (1.4 equiv) and sulfuric acid in a catalytic proportion were added, and the mixture was held for 1 h at 90 °C. Trifluoroacetic acid and all volatile impurities were removed with a rotavapor. Then, the product was added to a saturated solution of NaHCO₃ and extracted with ethyl acetate or another organic solvent and then evaporated. For the saponification, 600 mL of a solution of NaOH at 2 N containing 50 mL of ethanol was added to the

Scheme 2. Synthesis of the Monomers



product, and the mixture was held for 1 day at 100 °C. Then, 300 mL of the solution was removed with a rotavapor, and all organic impurities were removed by extraction with ethyl acetate. The solution was neutralized with hydrochloric acid 37% to pH 2, and the product precipitated. The product was recovered by filtration and washed with water. If the product does not precipitate, then the water is removed and the product is filtered and washed with water.

For $n = 6$ to 12. For the deprotection of the amine, the product was dissolved in 200 mL of trifluoroacetic acid. Then, anisole (1.4 equiv) and sulfuric acid in a catalytic proportion were added, and the mixture was held for 1 h at 90 °C. Trifluoroacetic acid and all volatile impurities were removed with a rotavapor. For saponification, 600 mL of a solution of NaOH at 2 N containing 50 mL of ethanol was added to the product, and the mixture was held for 1 day at 100 °C. Then, 300 mL of the solution was removed with a rotavapor, and the solution was neutralized with hydrochloric acid 37% to pH 2. Water was removed, and the product was filtered and washed with water.

Decarboxylation. To 100 mL of triethanolamine at 200 °C in a nitrogen atmosphere was added 3 g of the previously obtained product for about 1 to 2 min. Then, the product was extracted with ethyl acetate, and the solvent was evaporated. The product was purified by column chromatography using silica gel neutralized with triethylamine and using cyclohexane/ethyl acetate as the eluent.

3,4-Dimethoxy-1H-pyrrole (Py(OC₁)₂). Yield 32%, white crystalline solid with mp 95.5 °C. δ_{H} (200 MHz, CDCl₃): 7.03 (1 H, s), 6.22 (2 H, d), 3.76 (6 H, s). δ_{C} (200 MHz, CDCl₃): 138.15, 99.50, 58.45. FTIR (KBr): $\nu_{\text{max}}/\text{cm}^{-1}$ 3392, 3004, 2954, 1595, 1555, 1325, 1197, 1174, 742 cm^{-1} . MS (70 eV): m/z 127 (M⁺, 85), 112 (C₅H₆NO₂⁺, 100).

3,4-Diethoxy-1H-pyrrole (Py(OC₂)₂). Yield 27%, gray crystals with mp 40.0 °C. δ_{H} (200 MHz, CDCl₃): 7.03 (1 H, s), 6.22 (2 H, d), 3.93 (4 H, q), 1.38 (6 H, t). δ_{C} (200 MHz, CDCl₃): 137.14, 100.39, 66.75, 14.99. FTIR (KBr): $\nu_{\text{max}}/\text{cm}^{-1}$ 3379, 2982, 2901, 2875, 1585, 1550, 1479, 1323, 1185, 1145, 1047, 777, 737, 541 cm^{-1} . MS (70 eV): m/z 154.9 (M⁺, 56), 127 (C₆H₈NO₂⁺, 34), 98.9 (C₄H₅NO₂⁺, 100).

3,4-Dipropoxy-1H-pyrrole (Py(OC₃)₂). Yield 33%, dark crystals with mp 36.2 °C. δ_{H} (200 MHz, CDCl₃): 7.03 (1 H, s), 6.22 (2 H, d),

3.83 (4 H, t), 1.78 (4 H, m), 0.99 (6 H, t). δ_{C} (200 MHz, CDCl₃): 137.26, 100.55, 72.96, 22.54, 10.32. FTIR (KBr): $\nu_{\text{max}}/\text{cm}^{-1}$ 3377, 2965, 2936, 2875, 1585, 1550, 1475, 1326, 1186, 1147, 1044, 1004, 790, 738, 543 cm^{-1} . MS (70 eV): m/z 183 (M⁺, 36), 141.1 (C₇H₁₁NO₂⁺, 21), 99 (C₄H₅NO₂⁺, 100).

3,4-Dibutoxy-1H-pyrrole (Py(OC₄)₂). Yield 5%, dark crystals with mp 47.6 °C. δ_{H} (200 MHz, CDCl₃): 7.03 (1 H, s), 6.22 (2 H, d), 3.87 (4 H, t), 1.71 (4 H, m), 1.45 (4 H, m), 0.96 (6 H, t). δ_{C} (200 MHz, CDCl₃): 137.49, 100.71, 71.28, 31.5, 19.19, 13.87. FTIR (KBr): $\nu_{\text{max}}/\text{cm}^{-1}$ 3380, 3173, 3158, 2953, 2869, 1587, 1551, 1478, 1469, 1327, 1184, 1144, 733 cm^{-1} . MS (70 eV): m/z 211 (M⁺, 23), 98.9 (C₄H₅NO₂⁺, 100).

3,4-Bis(pentyloxy)-1H-pyrrole (Py(OC₅)₂). Yield 32%, dark crystals with mp 26.1 °C. δ_{H} (200 MHz, CDCl₃): 6.99 (1 H, s), 6.21 (2 H, d), 3.86 (4 H, t), 1.76 (4 H, m), 1.42 (8 H, m), 0.94 (6 H, t). δ_{C} (200 MHz, CDCl₃): 137.28, 100.50, 71.40, 28.93, 27.97, 22.30, 13.85. FTIR (KBr): $\nu_{\text{max}}/\text{cm}^{-1}$ 3406, 2956, 2932, 2871, 1586, 1546, 1323, 1185, 1138, 759 cm^{-1} . MS (70 eV): m/z 239.2 (M⁺, 95), 99.1 (C₄H₅NO₂⁺, 100).

3,4-Bis(hexyloxy)-1H-pyrrole (Py(OC₆)₂). Yield 28%, dark crystals with mp 48.3 °C. δ_{H} (200 MHz, CDCl₃): 7.01 (1 H, s), 6.21 (2 H, d), 3.86 (4 H, t), 1.76 (4 H, m), 1.41 (12 H, m), 0.92 (6 H, t). δ_{C} (200 MHz, CDCl₃): 137.23, 100.46, 71.40, 31.46, 29.20, 25.49, 22.44, 13.86. FTIR (KBr): $\nu_{\text{max}}/\text{cm}^{-1}$ 338, 3180, 3155, 2952, 2922, 2870, 1588, 1550, 1477, 1466, 1325, 1185, 1144, 789 cm^{-1} . MS (70 eV): m/z 267.2 (M⁺, 100), 99.1 (C₄H₅NO₂⁺, 92).

3,4-Bis(octyloxy)-1H-pyrrole (Py(OC₈)₂). Yield 5%, dark crystals with mp 55.2 °C. δ_{H} (200 MHz, CDCl₃): 6.97 (1 H, s), 6.21 (2 H, d), 3.85 (4 H, t), 1.79 (4 H, m), 1.34 (20 H, m), 0.88 (6 H, t). δ_{C} (200 MHz, CDCl₃): 137.30, 100.51, 71.44, 31.66, 29.26, 29.24, 29.1, 25.84, 22.49, 13.92. FTIR (KBr): $\nu_{\text{max}}/\text{cm}^{-1}$ 3380, 2922, 2852, 1590, 1550, 1466, 1326, 1186, 1145, 790 cm^{-1} . MS (70 eV): m/z 323.3 (M⁺, 92.5), 281.2 (C₁₇H₃₁NO₂⁺, 82.5), 207.1 (C₁₂H₁₇NO₂²⁺, 100).

3,4-Bis(decyloxy)-1H-pyrrole (Py(OC₁₀)₂). Yield 8%, white powder with mp 64.0 °C. δ_{H} (200 MHz, CDCl₃): 7.03 (1 H, s), 6.21 (2 H, d), 3.85 (4 H, t), 1.75 (4 H, m), 1.26 (20 H, m), 0.87 (6 H, t). δ_{C} (200 MHz, CDCl₃): 137.39, 100.61, 71.52, 31.79, 29.58, 29.51, 29.47, 29.34, 29.22, 25.90, 22.56, 13.98. FTIR (KBr): $\nu_{\text{max}}/\text{cm}^{-1}$ 3378, 2956, 2920, 2851,

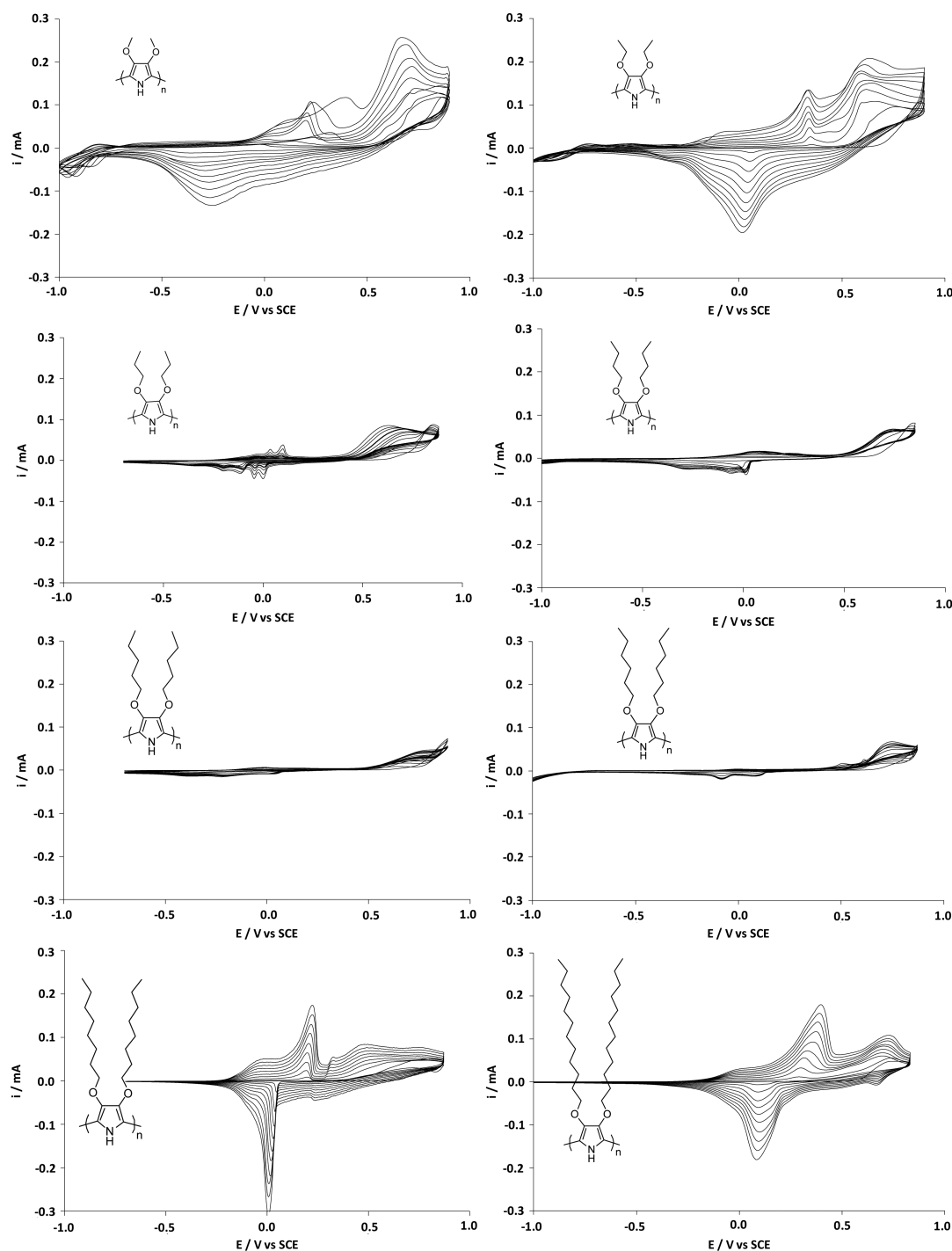


Figure 1. Ten scans of cyclic voltammetry of different monomers. Scan rate 20 mV s^{-1} .

1591, 1551, 1475, 1467, 1326, 1186, 1145, 791 cm^{-1} . MS (70 eV): m/z 379.4 (M^+ , 100), 281.2 ($\text{C}_{17}\text{H}_{31}\text{NO}_2^+$, 56), 238.2 ($\text{C}_{14}\text{H}_{24}\text{NO}_2^{2+}$, 48), 207.2 ($\text{C}_{12}\text{H}_{19}\text{NO}_2^+$, 69), 99.1 ($\text{C}_4\text{H}_5\text{NO}_2^+$, 76).

3,4-Bis(dodecyloxy)-1H-pyrrole (Py(OC₁₂)₂). Yield 5%, gray powder with mp 71.1°C . δ_{H} (200 MHz, CDCl_3): 6.97 (1 H, s), 6.21 (2 H, d), 3.85 (4 H, t), 1.75 (4 H, t), 1.24 (24 H, m), 0.87 (6 H, t). δ_{C} (200 MHz, CDCl_3): 137.26, 100.45, 71.39, 31.71, 29.47, 29.42, 29.32, 29.25, 29.22, 29.15, 25.80, 22.48, 13.91. FTIR (KBr): $\nu_{\text{max}}/\text{cm}^{-1}$ 3377, 2952, 2920.5, 2850, 1591, 1551, 1469, 1327, 1186, 114, 791 cm^{-1} .

Electrochemical Conditions. An Autolab potentiostat purchased from Metrohm was used for the electrodeposition experiments. The connection was realized via a three-electrode system. A platinum tip was used as a working electrode for cyclic voltammetry experiments,

a carbon rod was used as a counterelectrode, and a saturated calomel electrode (SCE) was used as a reference electrode. For the surface characterization, the polymers were electrodeposited on gold plates purchased from Neyco and consisted of a deposition of chromium (20 nm) and gold (150 nm) on a silicon wafer. The mean roughness (R_a) of the smooth gold plates is around 5 nm and has no significant influence on the surface wettability. In a glass cell connected to the potentiostat with the three-electrode system, 10 mL of anhydrous acetonitrile containing 0.1 M electrolytic salt and 0.01 M monomer were introduced under argon. First, the monomer oxidation potential (0.86–1.08 V vs SCE following the alkyl chain length of the monomer) was determined by cyclic voltammetry with the platinum tip as the working electrode. Multiple potential scans were performed to study the

polymer growth and to determine the polymer oxidation and reduction potentials. Then, polymer films were electrodeposited at constant potential on larger gold plates. Six depositions at constant potential were performed for each monomer at several deposition charges during the experiments: 12.5, 25, 50, 100, 200, and 400 mC cm^{-2} . Depositions at 1 mC cm^{-2} were also performed to prepared smooth polymer films. All polymer substrates were washed three times in acetonitrile to remove all remaining electrolyte and monomer.

Surface Characterization. Polymers were characterized by goniometry, scanning electron microscopy (SEM), and optical profilometry. The SEM images were recorded using a 6700F microscope (JEOL) at the CCMA (Centre Commun de Microscopie Appliquée, Univ. Nice Sophia Antipolis). The mean arithmetic (R_a) and quadratic (R_q) roughnesses were determined using a Wyko NT 1100 optical microscope (Bruker) with a 50 \times objective and a 0.5 \times field of view (FOV). VSI mode was used for smooth surfaces, and PSI mode was used for very rough surfaces. The apparent contact angles (θ) were measured using a DSA30 goniometer (Krüss) by taking the tangent at the triple-point contact line with a droplet of 2 μL . Milli-Q water (conductivity = 0.055 μS ; $\gamma_{\text{LV}} = 72.8$ mN/m), diiodomethane ($\gamma_{\text{LV}} = 50.0$ mN/m), and hexadecane ($\gamma_{\text{LV}} = 27.6$ mN/m) were used as probe liquids. For the dynamic contact angles, a 4 μL water droplet was placed on the substrate, and the substrate was inclined until the droplet moved. The advancing and receding contact angles are taken just before the droplet moves. The maximum inclination angle is called the sliding angle (α). If the droplet does not move even for $\alpha > 90^\circ$, then the hysteresis is extremely high and the substrate is called sticky.

The surface free energy (γ_{SV}) of the smooth surfaces and its dispersive ($\gamma_{\text{SV}}^{\text{D}}$) and polar ($\gamma_{\text{SV}}^{\text{P}}$) parts were determined using the Owens–Wendt equation: $\gamma_{\text{LV}}(1 + \cos \theta) = 2(\gamma_{\text{LV}}^{\text{D}} \gamma_{\text{SV}}^{\text{D}})^{1/2} + 2(\gamma_{\text{LV}}^{\text{P}} \gamma_{\text{SV}}^{\text{P}})^{1/2}$. Using three different liquids (water, diiodomethane, and hexadecane, for which γ_{LV} , $\gamma_{\text{LV}}^{\text{D}}$, and $\gamma_{\text{LV}}^{\text{P}}$ are known, $\gamma_{\text{SV}}^{\text{D}}$ and $\gamma_{\text{SV}}^{\text{P}}$ can be calculated by drawing the function $y = ax + b$ where $y = \gamma_{\text{LV}}(1 + \cos \theta)/2(\gamma_{\text{LV}}^{\text{D}})^{1/2}$ and $x = (\gamma_{\text{LV}}^{\text{P}})^{1/2}/(\gamma_{\text{LV}}^{\text{D}})^{1/2}$. Then, $\gamma_{\text{SV}}^{\text{D}} = b^2$ and $\gamma_{\text{SV}}^{\text{P}} = a^2$ are determined. In our case, $\gamma_{\text{SV}}^{\text{D}}$ and $\gamma_{\text{SV}}^{\text{P}}$ were directly obtained using the drop shape analysis software for our goniometer.

RESULTS AND DISCUSSION

Deposition Experiments. The electropolymerization experiments were performed in anhydrous acetonitrile containing 0.01 M monomer and 0.1 M salt used as an electrolyte. All monomers were perfectly soluble in acetonitrile except $\text{Py}(\text{OC}_{12})_2$, for which the monomer concentration is much less than 0.01 M. First, it was necessary to determine the monomer oxidation potential (E_m^{ox}) by cyclic voltammetry to know the intervals of tension where the monomer is reactive (oxidized). The monomer oxidation potential of each monomer (E_m^{ox}) using tetrabutylammonium perchlorate (Bu_4NClO_4) as the salt is the same for each monomer (between 0.89 and 0.93 V vs SCE), which indicates that the effect of the alkyl chain length is not very significant here.

Then, to study the polymer growth, multiple cyclic voltammetry experiments (10 scans) were performed between -1 V and E_m^{ox} . The cyclic voltammograms are shown in Figure 1 except for $\text{Py}(\text{OC}_{12})_2$ because its concentration was less than 0.01 M as a result of its low solubility. First, the intensity of the polymer oxidation and reduction peaks obtained with $\text{Py}(\text{OC}_3)_2$, $\text{Py}(\text{OC}_4)_2$, $\text{Py}(\text{OC}_5)_2$, and $\text{Py}(\text{OC}_6)_2$ is extremely low. Hence, these polymers have a high solubility in acetonitrile, which is problematic for obtaining stable and adherent polymer films. The intensity of the polymer oxidation and reduction peaks is high with $\text{Py}(\text{OC}_1)_2$ and $\text{Py}(\text{OC}_2)_2$, but the curves are not superposed after each scan, which indicates important steric hindrances. By contrast, when using long alkyl chains (≥ 8 carbons), extremely intense and well-defined cyclic voltammograms are obtained with a very nice superposition of each scan. Hence, the polymer oxidation and reduction potentials of these polymers do not evolve as the polymer thickness increases.

The effect of the alkyl chain length of the polymer solubility can be explained. First, it is expected that the polymer solubility

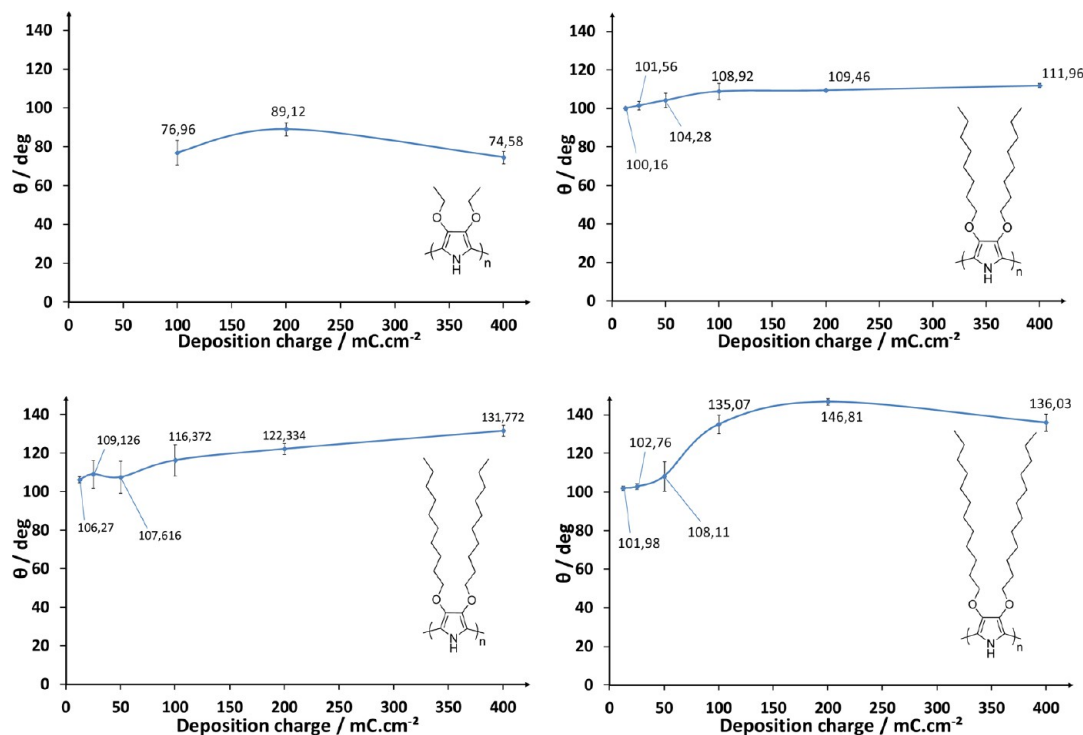


Figure 2. Apparent contact angle (θ) as a function of the deposition charge (Q_s) of the polymer ($\text{PPy}(\text{OC}_2)_2$, $\text{PPy}(\text{OC}_8)_2$, $\text{PPy}(\text{OC}_{10})_{10}$, and $\text{PPy}(\text{OC}_{10})_{12}$).

decreases when the length of the alkyl chain increases, which explains the high insolubility of $\text{Py}(\text{OC}_8)_2$, $\text{Py}(\text{OC}_{10})_2$, and $\text{Py}(\text{OC}_{12})_2$. However, the other important parameter influencing the polymer solubility is the polymer chain length. Here, because of steric hindrance, the polymer chain length is expected to increase when the length of the alkyl chain decreases, as observed by cyclic voltammetry (the polymer oxidation and reduction peaks decrease). Therefore, this is why the polymer insolubility is relatively important when for an alkyl chain length of $2 \leq n \leq 8$ whereas the polymer solubility is much more important for $3 \leq n \leq 6$.

Surface Wettability. Then, the polymers were electro-deposited on large gold plates at constant potential ($E = E^{\text{ox}}_{\text{m}}$) in order to evaluate the surface wettability and morphology. For the evaluation of the surface hydrophobicity of each polymer, goniometric measurements (θ_w) with water were performed as a function of the deposition charge (Q_s) at up to 400 mC cm^{-2} . As observed by cyclic voltammetry, $\text{PPy}(\text{OC}_3)_2$, $\text{PPy}(\text{OC}_4)_2$, $\text{PPy}(\text{OC}_5)_2$, and $\text{PPy}(\text{OC}_6)_2$ are too soluble in acetonitrile and the polymer film do not stay on the working electrode during the electrodeposition and washing treatments. This is also the case for $\text{PPy}(\text{OC}_1)_2$, $\text{PPy}(\text{OC}_2)_2$ films resist but only for high $Q_s \geq 100 \text{ mC cm}^{-2}$. By contrast, $\text{PPy}(\text{OC}_8)_2$, $\text{PPy}(\text{OC}_{10})_2$, and $\text{PPy}(\text{OC}_{12})_2$ are much more insoluble than all of the other polymers and could be electrodeposited whatever their Q_s .

The results on wettability and roughness are given in Figure 2 and Table 1. As expected, $\text{PPy}(\text{OC}_2)_2$ is hydrophilic. The surface

Table 1. Parameters for the Polymer Deposited at $Q_s = 100$, 200, and 400 mC cm^{-2} in NBU_4ClO_4

polymer	deposition charge [mC cm^{-2}]	θ_{water} [deg]	R_a [nm]	R_q [nm]
$\text{PPy}(\text{OC}_2)_2$	100	76.9	15	24
	200	89.1	26	35
	400	74.6	316	522
$\text{PPy}(\text{OC}_8)_2$	100	108.9	74	99
	200	109.5	116	147
	400	112.0	302	390
$\text{PPy}(\text{OC}_{10})_2$	100	116.4	103	206
	200	122.3	1626	2362
	400	131.8	1206	2150
$\text{PPy}(\text{OC}_{12})_2$	100	135.1	499	962
	200	146.8	4116	6822
	400	136.0	6225	6600

hydrophobicity increases and decreases with Q_s . The decrease in hydrophobicity between 200 and 400 mC cm^{-2} can be explained by a high increase in the surface roughness with the Wenzel equation. However, the increase in hydrophobicity between 100 and 200 mC cm^{-2} can be explained only by Cassie–Baxter and indicates the presence of a surface morphology able to trap air between the surface and the substrate.

$\text{PPy}(\text{OC}_8)_2$ is hydrophobic and θ_w is quite independent of Q_s even if the surface roughness increases. By contrast, for the longest alkyl chains ($n \geq 10$), θ_w increases with Q_s . A maximum value of 131.8° was reached with $\text{PPy}(\text{OC}_{10})_2$ for $Q_s = 400 \text{ mC cm}^{-2}$, and a value of 146.8° was reached with $\text{PPy}(\text{OC}_{12})_2$ for $Q_s = 200 \text{ mC cm}^{-2}$. Here, the polymer films are extremely rough, especially for $Q_s \geq 200 \text{ mC cm}^{-2}$. Moreover, the substrates are also extremely sticky. A water droplet placed on them remained stuck whatever the substrate inclination, as shown in Figure 3.

The SEM images (Figure 4) show an evolution of the surface morphology with the alkyl chain length. $\text{PPy}(\text{OC}_2)_2$ possess a

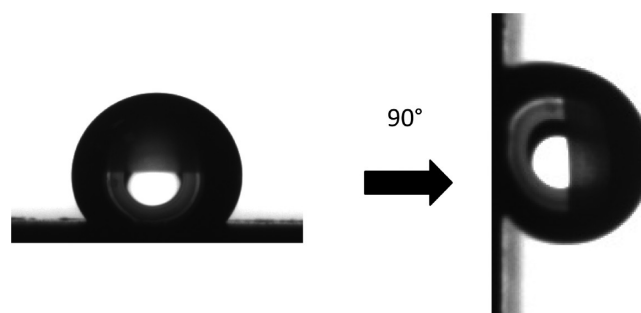


Figure 3. Picture of a water droplet deposited on $\text{PPy}(\text{OC}_{10})_2$ (200 mC cm^{-2}) before and after inclination at 90° .

fibrous morphology, which explains the possibility of increased hydrophobicity while the polymer is intrinsically hydrophilic by trapping a small amount of air between the surface and the droplet. $\text{PPy}(\text{OC}_8)_2$ presents an ordered nanodome systems, and $\text{PPy}(\text{OC}_{10})_2$ presents larger cauliflower-like structures. Hence, the presence of nanodomains is not sufficient to increase the surface hydrophobicity, but the presence of cauliflower-like structures greatly increases it. For $\text{PPy}(\text{OC}_{12})_2$, extremely large wrinkles are observed, which are often due to high tension in the films, but at the nanoscale the wrinkles are not highly structured. The presence of these large wrinkles explains the extremely high roughness obtained with the surfaces but also their high hydrophobicity.

The changes in the surface morphology from fibrous to cauliflower-like structures with the alkyl chain length can be easily explained. Indeed, it was shown in the literature that the surface morphology is highly affected by the solubility of the oligomers formed in the first instances of electropolymerization.⁶⁰ Here, the oligomers formed with $\text{Py}(\text{OC}_2)_2$ are highly soluble in acetonitrile, and two-dimensional growth is favored, leading to fibrous structures. By contrast, with very long alkyl chains, the oligomers are much more insoluble and spherical particles are obtained (three-dimensional growth).

Discussion. The results can be explained by the Wenzel and Cassie–Baxter equations.^{61,62} Indeed, these methods were developed to explain the wettability of rough surfaces. These equations are dependent on the Young angles (θ_w^Y),⁶³ which are the apparent contact angles of the same polymers but smooth, and it was first necessary to produce smooth surfaces. Here, the smooth polymers were obtained using an ultralow deposition charge of 1 mC cm^{-2} . Indeed, in the first instances of electropolymerization, a very thin layer of polymer covers all the substrate, but the surface structures have no time to grow. These θ_w^Y values can be found in Table 2, and roughness measurements confirmed their roughness.

$\text{PPy}(\text{OC}_8)_2$, $\text{PPy}(\text{OC}_{10})_2$, and $\text{PPy}(\text{OC}_{12})_2$ are intrinsically hydrophobic ($\theta_w^Y > 90^\circ$), and as expected, θ_w^Y increases and γ_{SV} decreases with the alkyl chain length. Here, the increase in the contact angle can now be explained by the Wenzel and Cassie–Baxter equations. With the Wenzel equation $\cos \theta_w = r \cos \theta_w^Y$, where r is a roughness parameter, it is possible to reach extremely high θ for only $\theta_w^Y > 90^\circ$, which is the case here.⁶⁰ However, with the Wenzel equation relatively important but not extremely high hysteresis is often predicted, as observed here. The Cassie–Baxter equation, with the presence of the air fraction between the surface and the water droplet, can allow this possibility.⁶¹ The Cassie–Baxter equation is $\cos \theta_w = r_f \cos \theta_w^Y + f - 1$, with r_f being the roughness ratio of the substrate wetted by the liquid, f being the solid fraction, and $(1 - f)$ being the air fraction.

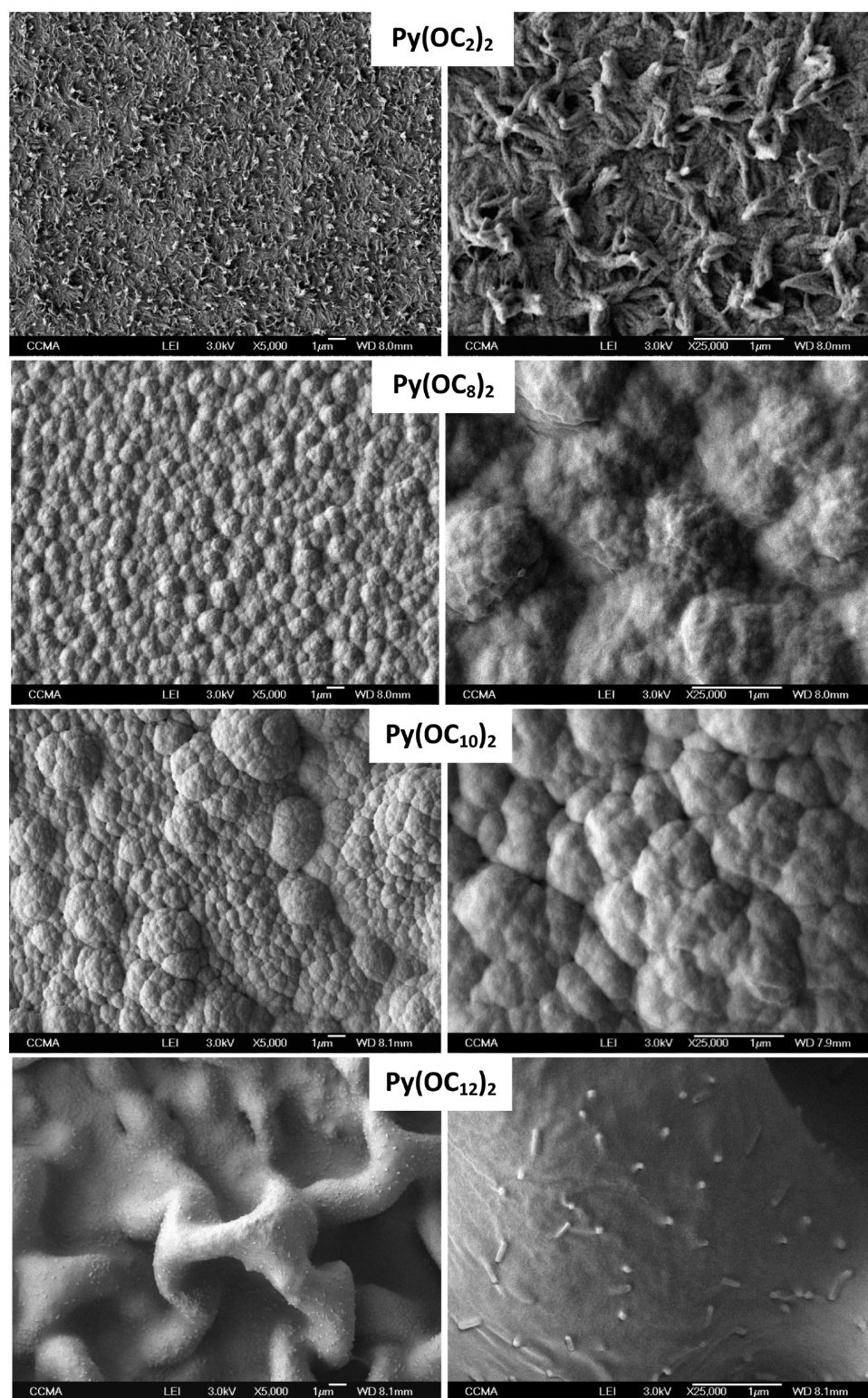


Figure 4. SEM images at two magnifications (5000 \times and 25 000 \times) of the different PPy(OC $_n$) $_2$ species ($Q_s = 200 \text{ mC cm}^{-2}$).

Table 2. Wettability and Roughness Parameters for the Smooth Polymer ($Q_s = 1 \text{ mC cm}^2$) Obtained in Bu $_4$ NClO $_4$

polymer	R_a [nm]	R_q [nm]	θ_w° [deg]	$\theta_{\text{diiodo}}^\circ$ [deg]	$\theta_{\text{hexadecane}}^\circ$ [deg]	γ_{SV} [mN m $^{-1}$]	γ_{SV}^D [mN m $^{-1}$]	γ_{SV}^P [mN m $^{-1}$]
PPy(OC $_8$) $_2$	5	6	96.7	50.2	0	31.08	30.19	0.88
PPy(OC $_{10}$) $_2$	6	12	103.2	49.1	17.4	30.53	30.39	0.14
PPy(OC $_{12}$) $_2$	6	8	105.7	58.5	26.3	27.27	27.16	0.11

With this equation, it is possible to predict ultralow water adhesion (superhydrophobic properties) if the air fraction is

very important but also extremely high water adhesion (parahydrophobic properties) if the air fraction is less important

or if θ_w^Y greatly decreases. Hence, the extremely high water adhesion of our surfaces is induced by the presence of nanodomains or cauliflower-like structures. When a water droplet is in contact with the surface, the solid–liquid interface is extremely important and the liquid–vapor interface is very low because the roughness of the surface structures is not fractal or hierarchical.

Other Experiments. Because $\text{Py}(\text{OC}_{10})_2$ gives extremely interesting results, other experiments were performed with this monomer. To modify both the surface morphology and hydrophobicity, other electrolytes were used: Bu_4NBF_4 , Bu_4NPF_6 , $\text{Bu}_4\text{NN}(\text{CF}_3\text{SO}_3)_2$, $\text{Bu}_4\text{NCF}_3\text{SO}_3$, $\text{Bu}_4\text{NC}_4\text{F}_9\text{SO}_3$, and $\text{Bu}_4\text{NC}_8\text{F}_{17}\text{SO}_3$. For each counterion, the same electrodeposition parameters were used. The cyclic voltammograms as a function of the electrolyte are given in Figure 5. These voltammograms show relatively similar curves using each electrolyte except for $\text{Bu}_4\text{NC}_8\text{F}_{17}\text{SO}_3$. It is not surprising to find different results with $\text{Bu}_4\text{NC}_8\text{F}_{17}\text{SO}_3$ because the films are stabilized by the counterions of the electrolyte and $\text{C}_8\text{F}_{17}\text{SO}_3^-$ counterions are much larger than the other ones, consequently inducing higher steric hindrance.

Then, the polymer films were also deposited at constant potential. Measurements of the water contact angles and roughness are given in Figures 6 and 7. SEM images are also

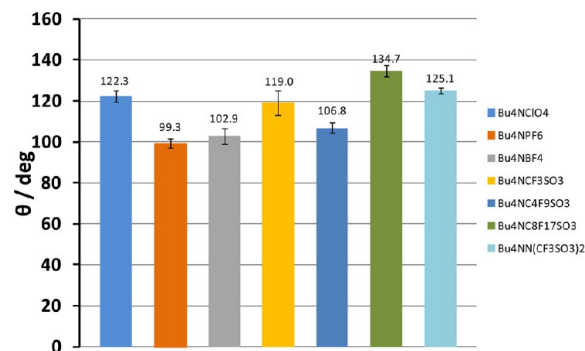


Figure 6. Graphic of water contact angles on $\text{PPy}(\text{OC}_{10})_2$ (200 mC cm^{-2}) using different electrolytes.

shown in Figures 8 and 9. Only two electrolytes ($\text{Bu}_4\text{NC}_8\text{F}_{17}\text{SO}_3$ and $\text{Bu}_4\text{N}(\text{CF}_3\text{SO}_3)_2$) induced a higher hydrophobicity than

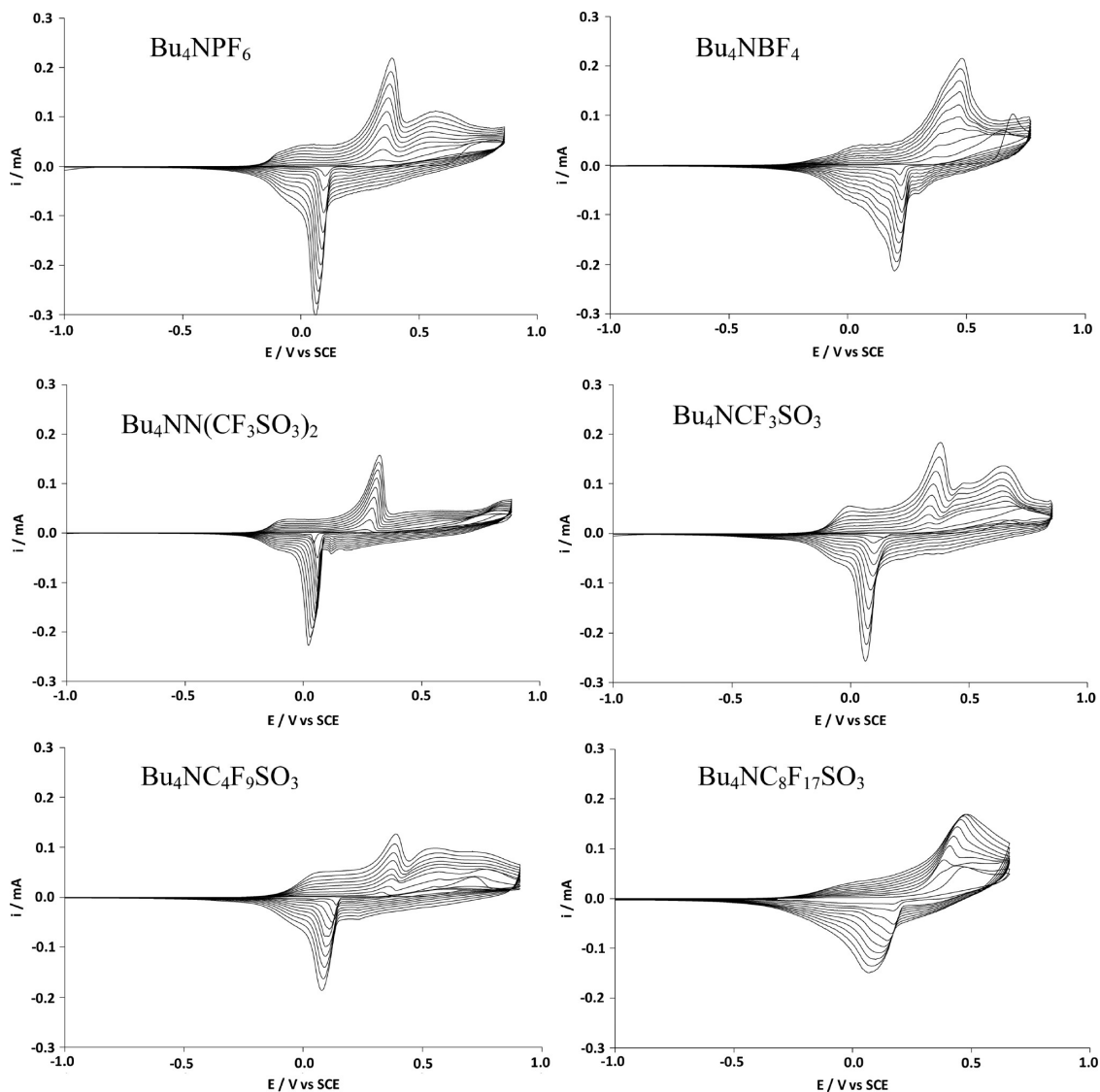


Figure 5. Ten cyclic voltammetry scans of $\text{PolyPy}(\text{OC}_{10})_2$ with different electrolytic salts. Scan rate 20 mV s^{-1} .

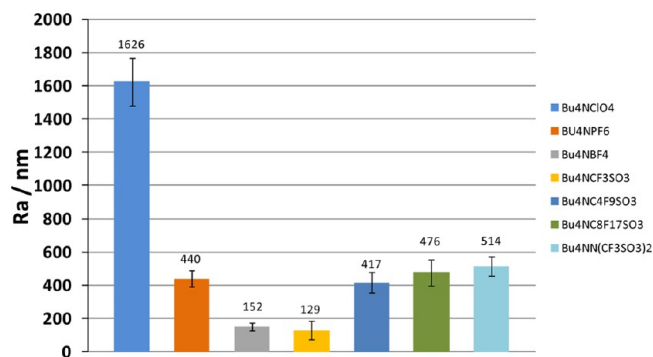


Figure 7. Graphic of roughness parameters on PPy(OC₁₀)₂ (200 mC cm⁻²) using different electrolytes.

did Bu₄NClO₄. Indeed, $\theta = 134.7$ and 125.1° , respectively, with Bu₄NC₈F₁₇SO₃ and Bu₄N(CF₃SO₃)₂.

SEM images as a function of the electrolyte are given in Figures 8 and 9. The electrolyte clearly impacts the surface

morphology and roughness. The films obtained with BF₄⁻ and C₄F₉SO₃⁻ are less rough as confirmed by profilometry measurements. For the deposition performed with PF₆⁻, C₈F₁₇SO₃⁻, C₄F₉SO₃⁻, and N(CF₃SO₃)₂⁻ there are the same mean roughnesses between 417 and 514 nm, but their roughness is much lower than with ClO₄⁻. The morphology is relatively similar in the presence of microdomes, but the number of domes as well as the presence of nanostructures is different with these electrolytes. This is sufficient to induce a significant change in surface hydrophobicity. It is strange that the surface hydrophobicity obtained with PF₆⁻ is lower than with ClO₄⁻ because the surface morphology is very similar. However, the mean roughness of the films obtained with ClO₄⁻ is much higher. To elucidate that, other SEM images were recorded but at a much lower magnification. As we can see in Figure 10, wrinkles are observed on these surfaces. The presence of wrinkles is more important with ClO₄⁻, which explains its high roughness and hydrophobicity.

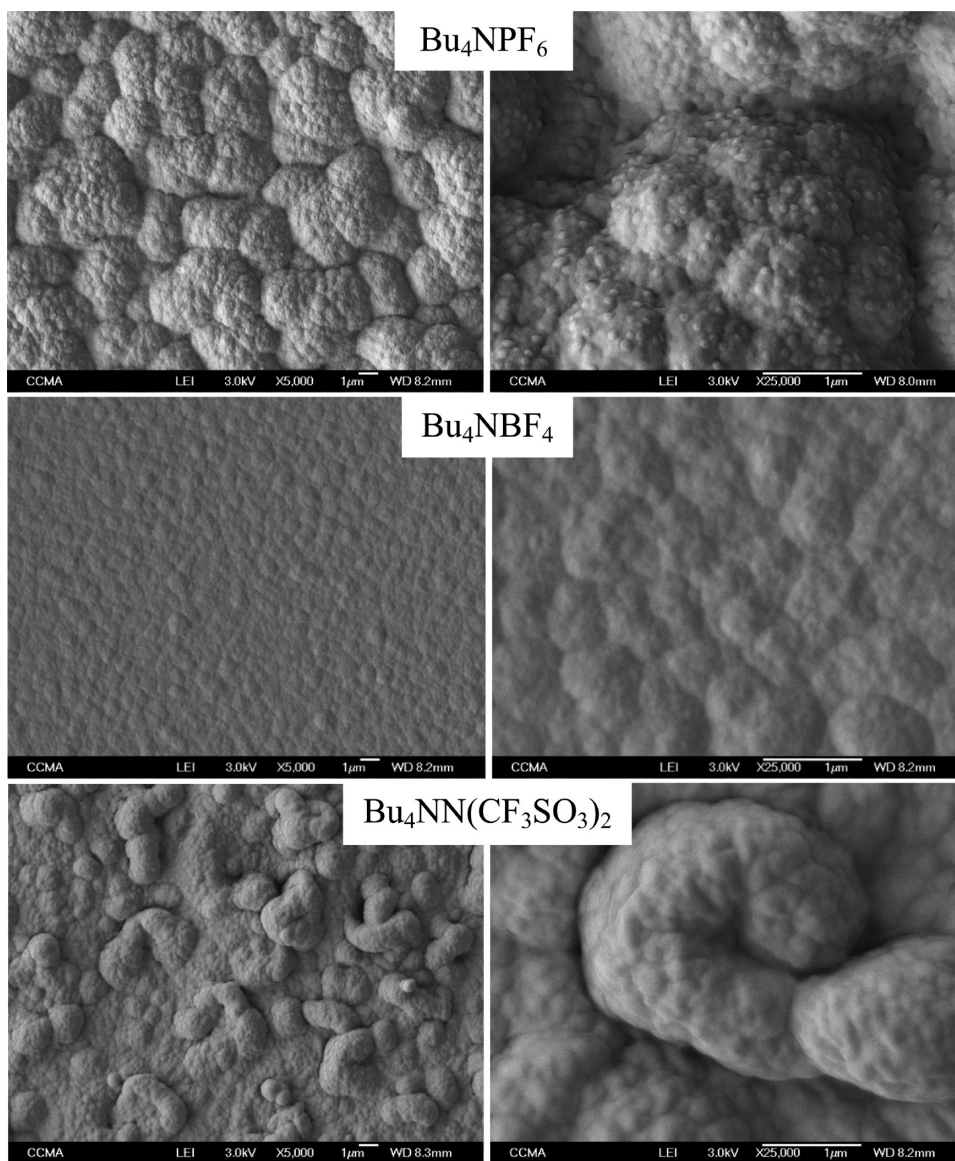


Figure 8. SEM images of PPy(OC₁₀)₂ ($Q_s = 200$ mC cm⁻²) at two magnifications (5000 \times and 25 000 \times) in different electrolytes: Bu₄NPF₆, Bu₄NBF₄, and Bu₄NN(CF₃SO₃)₂.

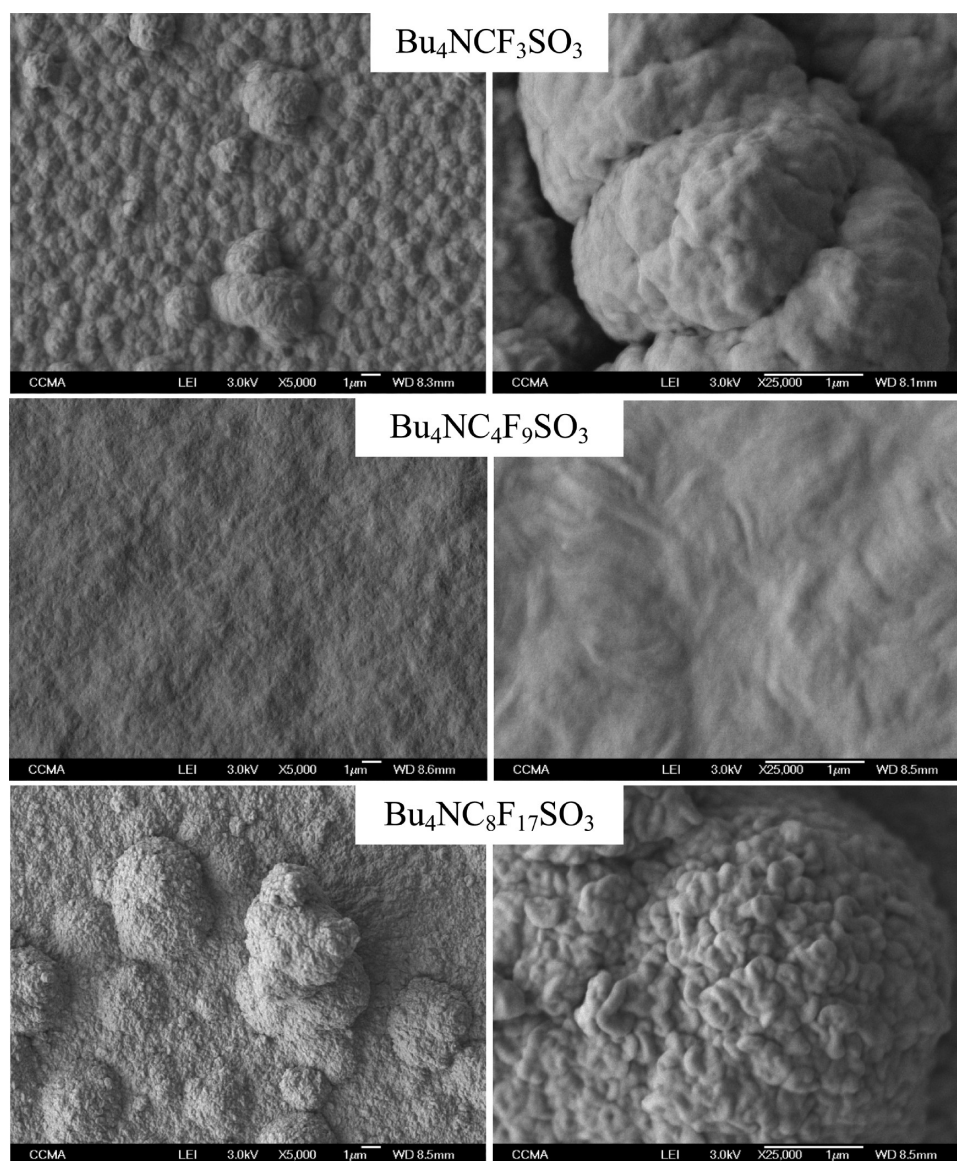


Figure 9. SEM images of $\text{Py}(\text{OC}_{10})_2$ ($Q_s = 200 \text{ mC cm}^{-2}$) at two magnifications (5000 \times and 25 000 \times) in different electrolytes: $\text{Bu}_4\text{NCF}_3\text{SO}_3$, $\text{Bu}_4\text{NC}_4\text{F}_9\text{SO}_3$, and $\text{Bu}_4\text{NC}_8\text{F}_{17}\text{SO}_3$.

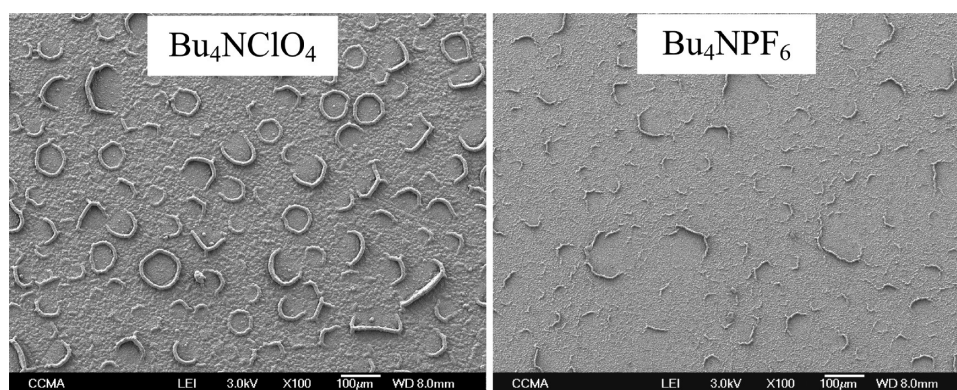


Figure 10. SEM images of $\text{Py}(\text{OC}_{10})_2$ ($Q_s = 200 \text{ mC cm}^{-2}$) at very low magnification (100 \times) in different electrolytes: Bu_4NClO_4 and Bu_4NPF_6 .

CONCLUSIONS

Here, we have synthesized pyrrole derivatives with two alkoxy groups of various lengths (from 1 to 12) in 8 steps by adapting a method developed by Merz et al., and we have used them to

develop parahydrophobic properties (high water adhesion) by electrodeposition. We showed that the alkyl chain length has a huge influence on the polymer solubility and as a consequence on the surface morphology and hydrophobicity. Moreover, the alkyl

chain length should be at least longer than eight carbons to obtain parahydrophobic properties. The properties were also controlled by the electrolyte nature. The materials have many potential applications in water harvesting and transportation or separation membranes, for example.

■ ASSOCIATED CONTENT

● Supporting Information

The Supporting Information is available free of charge on the ACS Publications website at DOI: 10.1021/acs.langmuir.6b02245.

¹H, ¹³C NMR, and mass spectra of Py compounds (PDF)

■ AUTHOR INFORMATION

Corresponding Author

*E-mail: frederic.guittard@unice.fr.

Notes

The authors declare no competing financial interest.

■ REFERENCES

- (1) Kimizuka, N.; Kawasaki, T.; Kunitake, T. Self-Organization of Bilayer Membranes from Amphiphilic Networks of Complementary Hydrogen Bonds. *J. Am. Chem. Soc.* **1993**, *115*, 4387–4388.
- (2) Kunitake, T. Synthetic Bilayer Membranes: Molecular Design, Self-organization, and Application. *Angew. Chem., Int. Ed. Engl.* **1992**, *31*, 1727–1746.
- (3) Darmanin, T.; Guittard, F. Recent Advances in the Potential Applications of Bioinspired Superhydrophobic Materials. *J. Mater. Chem. A* **2014**, *2*, 16319–16359.
- (4) Su, B.; Tian, Y.; Jiang, L. Bioinspired Interfaces with Superwettability: From Materials to Chemistry. *J. Am. Chem. Soc.* **2016**, *138*, 1727–1748.
- (5) Milionis, A.; Loth, E.; Bayer, I. S. Recent Advances in the Mechanical Durability of Superhydrophobic Materials. *Adv. Colloid Interface Sci.* **2016**, *229*, 57–79.
- (6) Lai, Y.; Huang, J.; Cui, Z.; Ge, M.; Zhang, K.-Q.; Chen, Z.; Chi, L. Recent Advances in TiO₂-Based Nanostructured Surfaces with Controllable Wettability and Adhesion. *Small* **2016**, *12*, 2203–2224.
- (7) Huang, J.-Y.; Lai, Y.-K.; Pan, F.; Yang, L.; Wang, H.; Zhang, K.-Q.; Fuchs, H.; Chi, L.-F. Multifunctional Superamphiphobic TiO₂ Nanostructure Surfaces with Facile Wettability and Adhesion Engineering. *Small* **2014**, *10*, 4865–4873.
- (8) Liu, M.; Zheng, Y.; Zhai, J.; Jiang, L. Bioinspired Super-antiwetting Interfaces with Special Liquid–Solid Adhesion. *Acc. Chem. Res.* **2010**, *43*, 368–377.
- (9) Liu, K.; Cao, M.; Fujishima, A.; Jiang, L. Bio-Inspired Titanium Dioxide Materials with Special Wettability and Their Applications. *Chem. Rev.* **2014**, *114*, 10044–10094.
- (10) Lai, Y.; Pan, F.; Xu, C.; Fuchs, H.; Chi, L. In Situ Surface-Modification-Induced Superhydrophobic Patterns with Reversible Wettability and Adhesion. *Adv. Mater.* **2013**, *25*, 1682–1686.
- (11) Koch, K.; Bhushan, B.; Barthlott, W. Multifunctional Surface Structures of Plants: An Inspiration for Biomimetics. *Prog. Mater. Sci.* **2009**, *54*, 137–178.
- (12) Sun, Z.; Liao, T.; Liu, K.; Jiang, L.; Kim, J. H.; Dou, S. X. Fly-Eye Inspired Superhydrophobic Anti-Fogging Inorganic Nanostructures. *Small* **2014**, *10*, 3001–3006.
- (13) Bush, J. W. M.; Hu, D. L.; Prakash, M. The Integument of Water-Walking Arthropods: Form and Function. *Adv. Insect Physiol.* **2007**, *34*, 117–192.
- (14) Su, Y.; Ji, B.; Zhang, K.; Gao, H.; Huang, Y.; Hwang, K. Nano to Micro Structural Hierarchy is Crucial for Stable Superhydrophobic and Water-Repellent Surfaces. *Langmuir* **2010**, *26*, 4984–4989.
- (15) Yu, Y.; Zhao, Z.-H.; Zheng, Q.-S. Mechanical and Superhydrophobic Stabilities of Two-Scale Surficial Structure of Lotus Leaves. *Langmuir* **2007**, *23*, 8212–8216.
- (16) Sarkar, A.; Kietzig, A.-M. Design of a Robust Superhydrophobic Surface: Thermodynamic and Kinetic Analysis. *Soft Matter* **2015**, *11*, 1998–2007.
- (17) Feng, L.; Zhang, Y.; Xi, J.; Zhu, Y.; Wang, N.; Xia, F.; Jiang, L. Petal Effect: A Superhydrophobic State with High Adhesive Force. *Langmuir* **2008**, *24*, 4114–4119.
- (18) Bhushan, B.; Nosonovsky, N. The Rose Petal Effect and the Modes of Superhydrophobicity. *Philos. Trans. R. Soc., A* **2010**, *368*, 4713–4728.
- (19) Lu, X.; Cai, H.; Wu, Y.; Teng, C.; Jiang, C.; Zhu, Y.; Jiang, L. Peach Skin Effect: A Quasi-Superhydrophobic State with High Adhesive Force. *Sci. Bull.* **2015**, *60*, 453–459.
- (20) Liu, K.; Du, J.; Wu, J.; Jiang, L. Superhydrophobic Gecko Feet with High Adhesive Forces towards Water and their Bio-Inspired Materials. *Nanoscale* **2012**, *4*, 768–772.
- (21) Sun, M.; Watson, G. S.; Zheng, Y.; Watson, J. A.; Liang, A. Wetting properties on nanostructured surfaces of cicada wings. *J. Exp. Biol.* **2009**, *212*, 3148–3155.
- (22) Yang, S.; Ju, J.; Qiu, Y.; He, Y.; Wang, H.; Dou, S.; Liu, K.; Jiang, L. (2014). Peanut Leaf Inspired Multifunctional Surfaces. *Small* **2014**, *10*, 294–299.
- (23) Osborn Popp, T. M.; Addison, J. B.; Jordan, J. S.; Damle, V. G.; Rykaczewski, K.; Chang, S. L. Y.; Stokes, G. Y.; Edgerly, J. S.; Yarger, J. L. Surface and Wetting Properties of Embiopteran (Webspinner) Nanofiber Silk. *Langmuir* **2016**, *32*, 4681–4687.
- (24) Marmur, A. Hydro- Hygro- Oleo- Omni-Phobic? Terminology of Wettability Classification. *Soft Matter* **2012**, *8*, 6867–6870.
- (25) Ju, J.; Bai, H.; Zheng, Y.; Zhao, T.; Fang, R.; Jiang, L. (2012). A Multi-Structural and Multi-Functional Integrated Fog Collection System in Cactus. *Nat. Commun.* **2012**, *3*, 1247.
- (26) Parker, A. R.; Lawrence, C. R. (2001). Water Capture by a Desert Beetle. *Nature* **2001**, *414*, 33–34.
- (27) Roth-Nebelsick, A.; Ebner, M.; Miranda, T.; Gottschalk, V.; Voigt, D.; Gorb, S.; Stegmaier, T.; Sarsour, J.; Linke, M.; Konrad, W. Leaf Surface Structures Enable the Endemic Namib Desert Grass *Stipagrostis Sabulicola* to Irrigate Itself with Fog Water. *J. R. Soc., Interface* **2012**, *9*, 1965–1974.
- (28) Shirtcliffe, N. J.; McHale, G.; Newton, M. I. Learning from Superhydrophobic Plants: The Use of Hydrophilic Areas on Superhydrophobic Surfaces for Droplet Control. *Langmuir* **2009**, *25*, 14121–14128.
- (29) Wu, D.; Wu, S.-Z.; Chen, Q.-D.; Zhang, Y.-L.; Yao, J.; Yao, X.; Niu, L.-G.; Wang, J.-N.; Jiang, L.; Sun, H.-B. Tip Curvature-Driven Reversible In Situ Switching Between Pinned and Roll-Down Superhydrophobic States for Water Droplet Transportation. *Adv. Mater.* **2011**, *23*, 545–549.
- (30) Heng, L.; Guo, T.; Wang, B.; Zhang, Y.; Jiang, L. Polymer Porous Interfaces with Controllable Oil Adhesion Underwater. *RSC Adv.* **2015**, *5*, 102378–102383.
- (31) Pinchasik, B.-E.; Steinkühler, J.; Wuytens, P.; Skirtach, A. G.; Fratzl, P.; Möhwald, H. From Beetles in Nature to the Laboratory: Actuating Underwater Locomotion on Hydrophobic Surfaces. *Langmuir* **2015**, *31*, 13734–13742.
- (32) Moradi, S.; Englezos, P.; Hatzikiriakos, S. G. Contact Angle Hysteresis of Non-Flattened-Top Micro/Nanostructures. *Langmuir* **2014**, *30*, 3274–3284.
- (33) Tsoi, S.; Fok, E.; Sit, J. C.; Veinot, J. G. C. Superhydrophobic, High Surface Area, 3-D SiO₂ Nanostructures Through Siloxane-Based Surface Functionalization. *Langmuir* **2004**, *20*, 10771–10774.
- (34) Li, Y.; Zheng, M.; Ma, L.; Zhong, M.; Shen, W. (2008). Fabrication of Hierarchical ZnO Architectures and Their Superhydrophobic Surfaces with Strong Adhesive Force. *Inorg. Chem.* **2008**, *47*, 3140–3143.
- (35) Szczepanski, C. R.; Darmanin, T.; Guittard, F. Spontaneous, Phase-Separation Induced Surface Roughness: A New Method to Design Parahydrophobic Polymer Coatings with Rose Petal-Like Morphology. *ACS Appl. Mater. Interfaces* **2016**, *8*, 3063–3071.

- (36) Utech, S.; Bley, K.; Aizenberg, J.; Vogel, N. Tailoring Re-Entrant Geometry in Inverse Colloidal Monolayers to Control Surface Wettability. *J. Mater. Chem. A* **2016**, *4*, 6853–6859.
- (37) Bao, B.; Sun, J.; Gao, M.; Zhang, X.; Jiang, L.; Song, Y. Patterning Liquids on Inkjet-Imprinted Surfaces with Highly Adhesive Superhydrophobicity. *Nanoscale* **2016**, *8*, 9556–9562.
- (38) Darmanin, T.; Guittard, F. Wettability of Conducting Polymers: From Superhydrophilicity to Superoleophobicity. *Prog. Polym. Sci.* **2014**, *39*, 656–682.
- (39) Li, C.; Bai, H.; Shi, G. Conducting Polymer Nanomaterials: Electrosynthesis and Applications. *Chem. Soc. Rev.* **2009**, *38*, 2397–2409.
- (40) McCarthy, C. P.; McGuinness, N. B.; Carolan, P. B.; Fox, C. M.; Alcock-Earley, B. E.; Breslin, C. B.; Rooney, A. D. Electrochemical Deposition of Hollow N-Substituted Polypyrrole Microtubes from an Acoustically Formed Emulsion. *Macromolecules* **2013**, *46*, 1008–1016.
- (41) Zhu, Y.; Hu, D.; Wan, M.; Jiang, L.; Wei, Y. Conducting and Superhydrophobic Rambutan-like Hollow Spheres of Polyaniline. *Adv. Mater.* **2007**, *19*, 2092–2096.
- (42) Fan, H.; Wang, H.; Guo, J.; Zhao, N.; Xu, J. Nanofibers-Based Nanoweb Promise Superhydrophobic Polyaniline: From Star-Shaped to Leaf-Shaped Structures. *J. Colloid Interface Sci.* **2013**, *409*, 255–258.
- (43) Xu, L.; Chen, W.; Mulchandani, A.; Yan, Y. Reversible Conversion of Conducting Polymer Films from Superhydrophobic to Superhydrophilic. *Angew. Chem., Int. Ed.* **2005**, *44*, 6009–6012.
- (44) Chiou, N.-R.; Lu, C.; Guan, J.; Lee, L. J.; Epstein, A. Growth and Alignment of Polyaniline Nanofibres with Superhydrophobic, Superhydrophilic and other Properties. *Nat. Nanotechnol.* **2007**, *2*, 354–357.
- (45) Gabriel, S.; Cécius, M.; Fleury-Frenette, K.; Cossement, D.; Hecq, M.; Ruth, N.; Jérôme, R.; Jérôme, C. Synthesis of Adherent Hydrophilic Polypyrrole Coatings onto (Semi)conducting Surfaces. *Chem. Mater.* **2007**, *19*, 2364–2371.
- (46) Yang, Y.; Li, S.; Zhang, L.; Xu, J.; Yang, W.; Jiang, Y. Vapor Phase Polymerization Deposition of Conducting Polymer/Graphene Nanocomposites as High Performance Electrode Materials. *ACS Appl. Mater. Interfaces* **2013**, *5*, 4350–4355.
- (47) Tarrade, J.; Darmanin, T.; Taffin de Givenchy, E.; Guittard, F.; Debarnot, D.; Poncin-Epaillard, F. Texturation and Superhydrophobicity of Polyethylene Terephthalate Thanks to Plasma Technology. *Appl. Surf. Sci.* **2014**, *292*, 782–789.
- (48) Darmanin, T.; Guittard, F. A One-Step Electrodeposition of Homogeneous and Vertically Aligned Nanotubes with Parahydrophobic Properties (High Water Adhesion). *J. Mater. Chem. A* **2016**, *4*, 3197–3203.
- (49) Darmanin, T.; Diouf, A.; El-Maïss, J.; Dieng, S. Y.; Guittard, F. Control over Water Adhesion of Nanostructured Parahydrophobic Films using Mesh Substrates. *ChemNanoMat* **2015**, *1*, 497–501.
- (50) Walczak, R. M.; Reynolds, J. R. Poly(3,4-alkylenedioxyppyroles): The PxDOPs as Versatile Yet Underutilized Electroactive and Conducting Polymers. *Adv. Mater.* **2006**, *18*, 1121–1131.
- (51) Schottland, P.; Zong, K.; Gaupp, C. L.; Thompson, B. C.; Thomas, C. A.; Giurgiu, I.; Hickman, R.; Abboud, K. A.; Reynolds, J. R. Poly(3,4-alkylenedioxyppyrole)s: Highly Stable Electronically Conducting and Electrochromic Polymers. *Macromolecules* **2000**, *33*, 7051–7061.
- (52) Zong, K.; Reynolds, J. R. 3,4-Alkylenedioxyppyroles: Functionalized Derivatives as Monomers for New Electron-Rich Conducting and Electroactive Polymers. *J. Org. Chem.* **2001**, *66*, 6873–6882.
- (53) Cho, Y.; Pyo, M.; Zong, K. Chemical and Electrochemical Synthesis of Highly Conductive and Processable PolyProDOP-alkyl Derivatives. *J. Korean Electrochem. Soc.* **2010**, *13*, 57–62.
- (54) Walczak, R. M.; Jung, J.-H.; Cowart, J. S., Jr.; Reynolds, J. R. 3,4-Alkylenedioxyppyrole-Based Conjugated Polymers with Finely Tuned Electronic and Optical Properties via a Flexible and Efficient N Functionalization Method. *Macromolecules* **2007**, *40*, 7777–7785.
- (55) Darmanin, T.; Guittard, F. Molecular Design of Conductive Polymers to Modulate Superoleophobic Properties. *J. Am. Chem. Soc.* **2009**, *131*, 7928–7933.
- (56) Darmanin, T.; Guittard, F. Enhancement of the Superoleophobic Properties of Fluorinated PEDOP using Polar Glycol Spacers. *J. Phys. Chem. C* **2014**, *118*, 26912–26920.
- (57) Mortier, C.; Darmanin, T.; Guittard, F. A Bioinspired Approach to Produce Parahydrophobic Properties using PEDOP Conducting Polymers with Branched Alkyl Chains. *Pure Appl. Chem.* **2015**, *87*, 805–814.
- (58) Mortier, C.; Darmanin, T.; Guittard, F. 3,4-Ethylenedioxyppyrole (EDOP) Monomers with Aromatic Substituents for Parahydrophobic Surfaces by Electropolymerization. *Macromolecules* **2015**, *48*, 5188–5195.
- (59) Merz, A.; Schropp, R.; Doetterl, E. 3,4-Dialkoxyppyroles and 2,3,7,8,12,13,17,18-Octaalkoxyppyryrins. *Synthesis* **1995**, *1995*, 795–800.
- (60) Poverenov, E.; Li, M.; Bitler, A.; Bendikov, M. Major Effect of Electropolymerization Solvent on Morphology and Electrochromic Properties of PEDOT Films. *Chem. Mater.* **2010**, *22*, 4019–4025.
- (61) Wenzel, R. N. Resistance of Solid Surfaces to Wetting by Water. *Ind. Eng. Chem.* **1936**, *28*, 988–994.
- (62) Cassie, A. B. D.; Baxter, S. Wettability of Porous Surfaces. *Trans. Faraday Soc.* **1944**, *40*, 546–551.
- (63) Young, T. An Essay on the Cohesion of Fluids. *Philos. Trans. R. Soc. London* **1805**, *95*, 65–87.